Kaliotoxin (1−37) Shows Structural Differences with Related Potassium Channel Blockers†

I. Fernández,‡ R. Romi,§ S. Szendeffy,‡,|| M. F. Martin-Eauclaire,§ H. Rochat,§ J. Van Rietschoten,§ M. Pons,*,‡ and E. Giralt‡

Department of Organic Chemistry, University of Barcelona, Martí i Franqués 1-11, Barcelona 08028, Spain, and Laboratoire d'Ingénierie des Protéines, URA 1455, Centre National de la Recherche Scientifique, Faculté de Médecine, Marseille, France

Received July 27, 1994; Revised Manuscript Received September 19, 1994⊗

ABSTRACT: The three-dimensional structure of kaliotoxin (1−37), KTX(1−37), a toxin from the scorpion *Androctonus mauretanicus mauretanicus* that blocks calcium-dependent potassium channels, has been determined by NMR. This toxin is homologous with other scorpion toxins such as charybdotoxin (ChTX) or iberiotoxin (IbTX) for which the structures are already known, but the presence of prolines in the expected α-helical region suggested that there may be some major difference in the structure of KTX that could be related to its different selectivity. Proline residues are also found in the homologous region of other scorpion toxins such as noxiustoxin or margatoxin. Our results indicate that KTX(1−37) contains the same sequence of secondary structure elements as ChTX but that the helical region is shorter and distorted due to the presence of two prolines. The distortion consists of a bending in the α-helix and in the presence of a 3_{10} helix turn in the last three residues. Furthermore, the increased length of the extended structure preceding the helix favors a different packing of this part of the molecule with respect to the secondary structure elements. This change in folding modifies the accessibility of the conserved ^{27}Lys which is known, from mutation studies, to be involved in channel blocking by ChTX.

Kaliotoxin (KTX)[1] is a peptide (38 residues, 3 disulfide bridges) isolated from the venom of the scorpion *Androctonus mauretanicus mauretanicus* (Crest et al., 1992). This toxin acts as an inhibitor of the high-conductance Ca^{2+}-activated K^+ channels (BKCa) of mollusc neurons as well as an inhibitor of the A-type voltage sensitive K^+ channel of rat brain.

KTX shows important sequence homology with other known scorpion toxins such as charybdotoxin (ChTX) (Gimenez-Gallego et al., 1988; Sugg et al., 1990), iberiotoxin (IbTX) (Galvez et al., 1990), noxiustoxin (NTX) (Possani et al., 1982), and margatoxin (MgTX) (García-Calvo et al., 1993). In particular, it has a conserved disulfide bridge pattern and a cluster of 10 conserved amino acid residues from position 26 to 35 in KTX sequence including four positively charged residues (Figure 1). For the two related toxins whose 3D structure is already known (ChTX and IbTX) (Bontems et al., 1991, 1992) (Johnson et al., 1992), this sequence similarity has resulted in a very similar folding

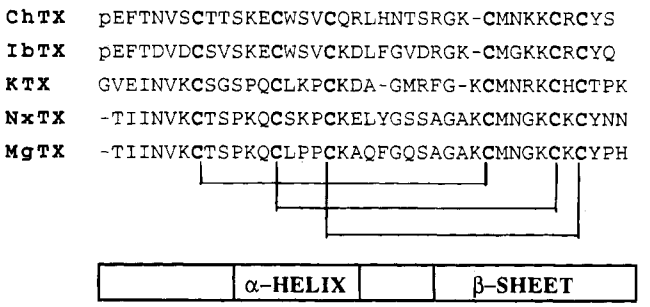

FIGURE 1: Sequence homology between KTX and other scorpion toxins: ChTX = charybdotoxin; IbTX = iberiotoxin; NTX = noxiustoxin; MgTX = margatoxin. The extension of the secondary structure elements indicated corresponds to the one found in KTX.

pattern characterized by an antiparallel β-sheet spanning the C-terminal part of the molecule (residues 26−35 in ChTX and 25−36 in IbTX) and an α-helix comprising residues 10 to 20 in ChTX and 13 to 21 in IbTX. The helical part includes a Cys-X-X-X-Cys pattern with both Cys residues forming disulfide bonds to a Cys-X-Cys sequence in the β-sheet. This cystine-stabilized helical motif has also been identified in α and β scorpion toxins such as AaH II from *Androctonus australis Hector* (Fontecilla-Camps et al., 1988) and CsEv3 from *Centruroides sculpturatus Ewing* (Fontecilla-Camps et al., 1980). It has been suggested that it may play a crucial function bringing into juxtaposition specific residues involved in binding the toxins to the channel protein (Kobayashi et al., 1991).

Despite these fundamental similarities in channel modulation properties, there are quantitative differences in their specific interactions. For example, KTX specifically suppresses the mollusc cell Ca^{2+}-activated K^+ current but has few detectable effects on Ca^{2+}-activated K^+ current at a

† Supported by Grants PB91-283 and PB92-0864 from DGICYT and by a predoctoral fellowship from Ministerio de Educación y Ciencia (to I.F.).

‡ University of Barcelona.

§ Laboratoire d'Ingénierie des Protéines.

|| Present address: University of Eötvös Lòrand (Budapest).

⊗ Abstract published in *Advance ACS Abstracts,* November 1, 1994.

[1] Abbreviations: ChTX, charybdotoxin; IbTX, iberiotoxin; KTX, kaliotoxin; NTX, noxiustoxin; MgTX, margatoxin; 3D structure, tridimensional structure; NMR, nuclear magnetic resonance; NOE, nuclear Overhauser effect; TOCSY, two-dimensional total correlation spectroscopy; DQF-COSY, two-dimensional double-quantum-filtered correlation spectroscopy; NOESY, two-dimensional nuclear Overhauser effect spectroscopy; ppm, parts per million; d(Hαi-HNi+1), (d_{NN}, $d_{\alpha N(i,i+3)}$), etc., intramolecular distance between protons CαH of residue i and NH of residue i+1, between NH and NH, between protons CαH of residue i and NH of residue i+3; $^3J_{HN\text{-}H\alpha}$, coupling constant between NH proton and CαH proton; CSI, chemical shift index.

0006-2960/94/0433-14256$04.50/0

mammalian motor nerve terminal (Harvey et al., 1994) unlike the other two related toxins (ChTX and IbTX) which show the same activity on both systems. It has been shown that ChTX and IbTX bind in a similar manner; this may be different for KTX; therefore, the study of the 3D structure of KTX can be a useful tool to identify common structural elements involved in interfering with neurotransmission at the ion channel level and structural features responsible for their different selectivities in various channels.

The presence of two Pro residues in the highly conserved helical region is a major difference between KTX and IbTX or ChTX. NTX and MgTX also present a conserved Pro residue in position X_3 of the helical Cys-$X_1X_2X_3$-Cys motif and a second Pro in position i-2 or i-3 with respect to the same motif and also in a region which is helical in both IbTX and ChTX. MgTX has a third Pro in position X_2. Recently, a toxin from *Tityus serrulatus* (TsTx-Kα) has also been shown to present two prolines in its supposedly α-helical part (Rogowski et al., 1994). The conservation of these Pro residues suggests that they may have a functional role, perhaps in determining a different selectivity.

The present study has been carried out with KTX(1−37) differing from the natural toxin by the deletion of a Lys residue at the C-terminus. This peptide is biochemically well characterized (Crest et al., 1992; Romi et al., 1993) and shows a slightly enhanced activity compared to the natural toxin as blocker of the Ca^{2+}-activated K^+ channels.

MATERIALS AND METHODS

Sample Preparation. KTX(1−37) was prepared by solid-phase peptide synthesis, purified, and characterized as previously described (Romi et al., 1993) . The pattern of disulfides was established by enzymatic hydrolysis and was confirmed by the NMR data described below. All NMR measurements were performed in a sample containing 8 mg of KTX(1−37) dissolved in 500 μL of 85% H_2O + 15% D_2O (3 mM), (pH = 3.27); after a set of NMR experiments, this sample was lyophilized and dissolved in pure D_2O. Dioxane was used as internal reference.

NMR Measurements. All NMR measurements were performed on a Varian VXR500 spectrometer. Spin system identification and sequential assignments were achieved by analysis and comparison of two-dimensional TOCSY (Braunschweiler et al., 1983; Davis et al., 1985), DQF-COSY (Rance et al., 1983), and NOESY (Jeener et al., 1979; Macura et al., 1981) experiments in H_2O and D_2O at 35 and 25 °C. TOCSY spectra were recorded with a spin-lock time of 80 ms. Three mixing times (100, 200, and 400) were used for NOESY in order to identify spin-diffusion effects. The NOESY mixing time was varied randomly by 10% to minimize the contribution from zero-quantum coherences. Analysis of the spin coupling constants was carried out using DQF-COSY in 15% and 100% D_2O at 35 °C (Rance et al., 1983). Presaturation was used to suppress water in all these experiments.

All two-dimensional data matrices (512 blocks of 64 scans) were zero-filled in both dimensions to obtain 4096 × 2048 time−domain data points and were multiplied by a shifted sine-bell in both dimensions prior to Fourier transformation. Processing and analysis of the spectra were carried out using Varian VNMR software.

Proton−deuterium exchange of amide groups was studied on a sample of KTX(1−37) lyophilized from H_2O and dissolved in pure D_2O. The disappearance of NH signals was followed at 30 °C. The first spectrum was acquired within 5 min of the dissolution of the sample. One-dimensional spectra were acquired every 10 min over the first 2 h. Then a 2D DQF-COSY spectrum, taking about 7 h, was acquired.

Structure Calculations. The determination of structures consistent with the experimental data was carried out using a combination of distance geometry (DGII program) (Havel, 1983) with simulated annealing (Discover program) (Feinstein et al., 1991) calculations. Both programs are implemented in the NMR-Chitect package commercially available from Biosym.

NOE intensities were classified in three groups (weak, medium, strong) by estimating the intensities of the cross-peaks in spectra recorded at 25 and 35 °C. The lower bound for all constraints was 1.9 Å. The upper bound was 2.2 Å for strong d(Hαi-HNi+1), 2.8 Å for strong d(HNi-HNi+1), 3.5 Å for medium, and 4.0 Å for weak intensity peaks. In addition, cross-peaks only detected in NOESY spectra acquired with longer mixing times, and which could not be attributed to an easily identified spin-diffusion pathway, were included as "very weak" constraints corresponding to an upper bound of 5 Å. To allow for molecular motion in the calculated bounds, an extra 0.5 Å was added to all upper bounds for NOE constraints involving side-chain atoms. Pseudoatoms were used where diastereotopic protons could not be distinguished from each other and the corresponding corrections for restraints involving pseudoatoms were applied (Wüthrich, 1986).

The ϕ dihedral angle constraints were derived from $^3J_{HN\text{-}H\alpha}$ coupling constants, ϕ angles were constrained to −120° ± 15° if $^3J_{HN\text{-}H\alpha} > 9$ Hz, to −120° ± 30° if 9 Hz > $^3J_{HN\text{-}H\alpha} > 8$ Hz, and to −70° ± 30° if $^3J_{HN\text{-}H\alpha} < 6$ Hz.

Molecular Modeling Calculations. A putative structure for KTX(1−37) was generated independently from the NMR data by searching the energy hypersurface starting from the known structure of ChTX (Bontems et al., 1991). Alignment of the two sequences was made on the basis of the disulfide bond pattern and the suggested conservation of ^{26}Gly. Side chains were mutated gradually starting with the residues located at the surface. After each mutation the structure was minimized. At three stages during the mutation protocol the structure was subjected to a molecular dynamics annealing and extensive minimization. The final mutated structure was minimized in a water box until the maximum derivative was lower than 0.01 kcal/mol. The full mutation protocol is the following: ^{31}K^{31}R/^{14}W^{15}L/ ^{8}T^{9}S, ^{12}E^{13}Q, ^{18}Q^{19}K, ^{20}L^{21}A, ^{34}R^{34}H//^{1}Z^{2}V, ^{2}F^{3}E, ^{9}T^{10}G, ^{11}K^{12}P, ^{36}Y^{36}T, ^{37}S^{37}P/--^{1}G, ^{3}T^{4}I/,^{23}T^{23}M/ ^{21}H--, ^{22}N^{22}G//^{6}S^{7}K, ^{15}S^{16}K, ^{19}R^{20}E, ^{25}R^{25}F/ ^{16}V^{17}P, ^{24}S^{24}R//. In each pair the first residue (represented in one letter code) is from ChTX and the second from KTX-(1−37), Z stands for pyroglutamic acid, and dashes indicate a residue not present in the corresponding toxin and that has been added or deleted accordingly. Slashes indicate minimization stages. Double slashes indicate molecular dynamics annealing.

The electrostatic potentials were calculated by integrating the Poisson-Boltzmann equation using the finite increment method as implemented in the Delphi program (Biosym) (Gilson et al., 1988). Formal unitary charges were located in the appropriate side chains, and the potential was calculated at the boundary of the solvent accessible surface

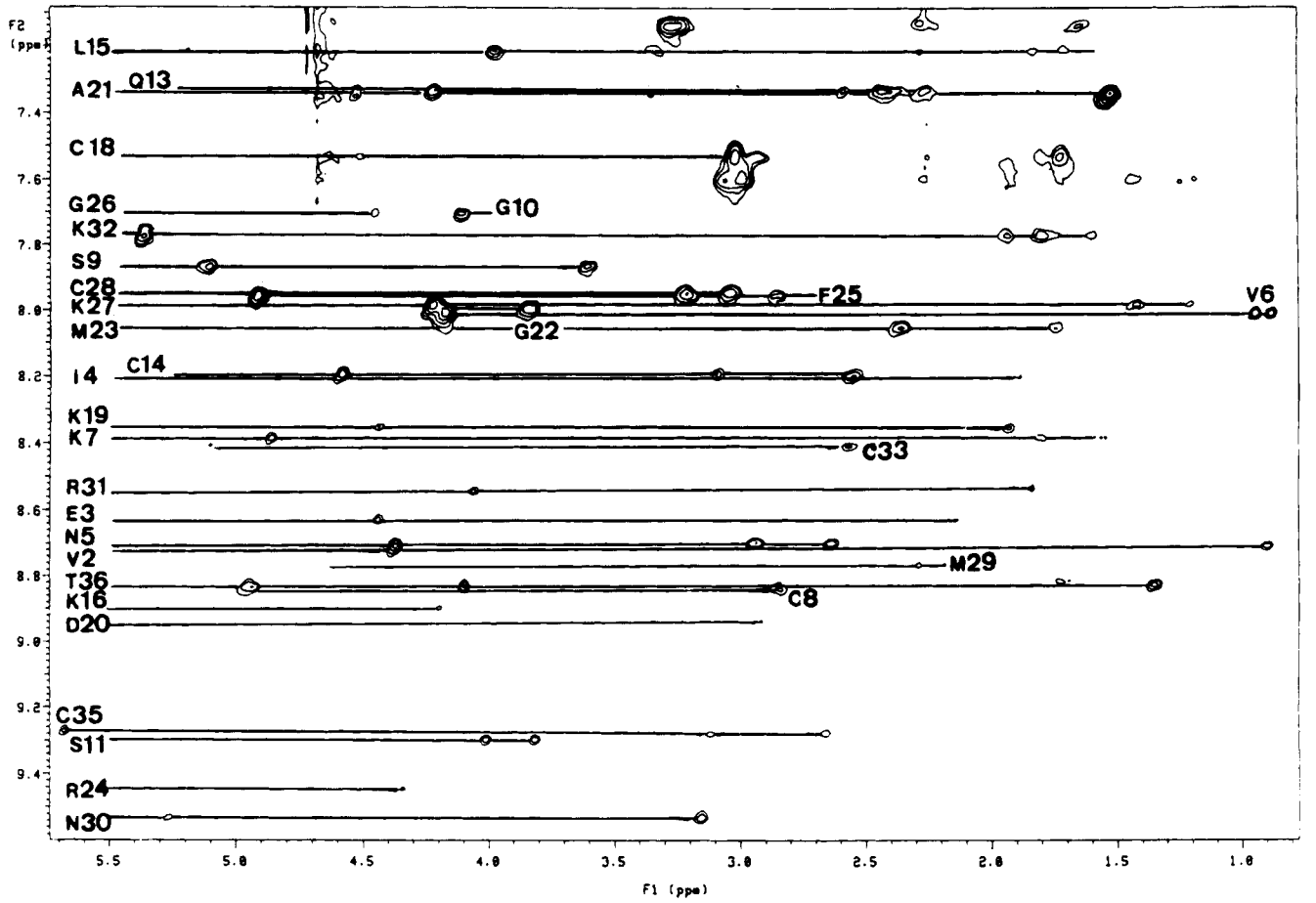

FIGURE 2: TOCSY spectrum of KTX(1−37) 3 mM in 85% H_2O−15% D_2O at 35 °C and pH = 3.27 (electrode reading).

determined according to the Connolly algorithm using a sphere with a radius of 2 Å as a probe.

RESULTS

Sequential Assignments. Cross-peaks between HN and CH_α protons were identified by examination of DQF-COSY spectra acquired in H_2O. TOCSY spectra were used to correlate side-chain spin systems with the NH-CH_α cross-peaks (Figure 2). By combining the information from TOCSY experiments performed at two temperatures (25 and 35 °C) all the NH-CH_α connectivities could be identified.

NOESY cross-peaks correlating sequentially adjacent residues (HN_i-HN_{i+1}(d_{NN}), $H_{\alpha i}$-HN_{i+1}($d_{\alpha N}$), and $H_{\beta i}$-HN_{i+1}-($d_{\beta N}$)) were used to assign spin systems to specific residues in the KTX(1−37) sequence. The single isoleucine, leucine, alanine, and threonine residues provided useful markers for the sequential assignments. A series of strong $d_{\alpha N}$ characterize the regions 2−7, 23−26 and 30−37. As can be seen from Figure 3, a series of d_{NN} connectivities were observed for regions 10−11, 13−16, and 18−22. The chemical shifts of all protons of kaliotoxin(1−37) are listed on Table 1.

Secondary Structure. The pattern of short- and medium-range NOEs (d_{NN}, $d_{\alpha N(i,i+3)}$, and $i,i+4$) and $^3J_{HN\text{-}H\alpha}$ coupling constants smaller than 6 Hz (Figure 4), together with slow rates of HN-DN exchange, is characteristic of a helix formed by residues 12−20. Further experimental support for the existence of the helix is provided by the negative Hα conformational shifts (Ösapay et al., 1991) (−0.1, −0.5 ppm) observed for the residues in this region (Figure 5).

The pattern of NOEs seen in the region of residues 25−37 is consistent with that expected for an antiparallel β-sheet in a hairpin structure: the 22−28 and 33−37 short strands show the characteristic large $^3J_{HN\text{-}H\alpha}$ coupling constants and a pattern of long-range NOEs between the two strands that demonstrate their antiparallel topology. The protons showing slow rates of exchange with deuterons are those expected to be hydrogen bonded in this sheet. Residues 29−32 join the two strands by a turn (sequential dNN and $d\alpha$N suggest that might be a type I β-turn). Large positive Hα conformational shifts (0.2, 1.0 ppm) are observed for residues 25−26 and 28−37.

Tertiary Structure. The data base used to derive the tertiary structure contained a total of 133 interresidue NOE constraints, including 71 short-range and 62 medium- and long-range. The short-range NOE constraints included 23 anti-NOEs that were introduced as distances longer than 3 Å. Experimentally, those correspond to the absence of a cross-peak which can be unequivocally established in some well-resolved spectral regions. These anti-NOEs were used in the initial search of the conformational space but were removed in the refinement of the final structure. In addition to these, 20 dihedral angle constraints, 7 hydrogen bond constraints, 9 restraints for the three disulfide bridges (Srinivasan et al., 1990), and 12 stereospecific assignments were used.

After a series of preliminary runs, three sets of 50 independently generated structures were obtained depending on the presence and type of hydrogen bond restraints used in the helical part of the molecule. In the first set no hydrogen bonds were assumed in the helical part of the molecule. In the second set all NH protons from residues 12 to 20 showing slow H−D exchange were considered to

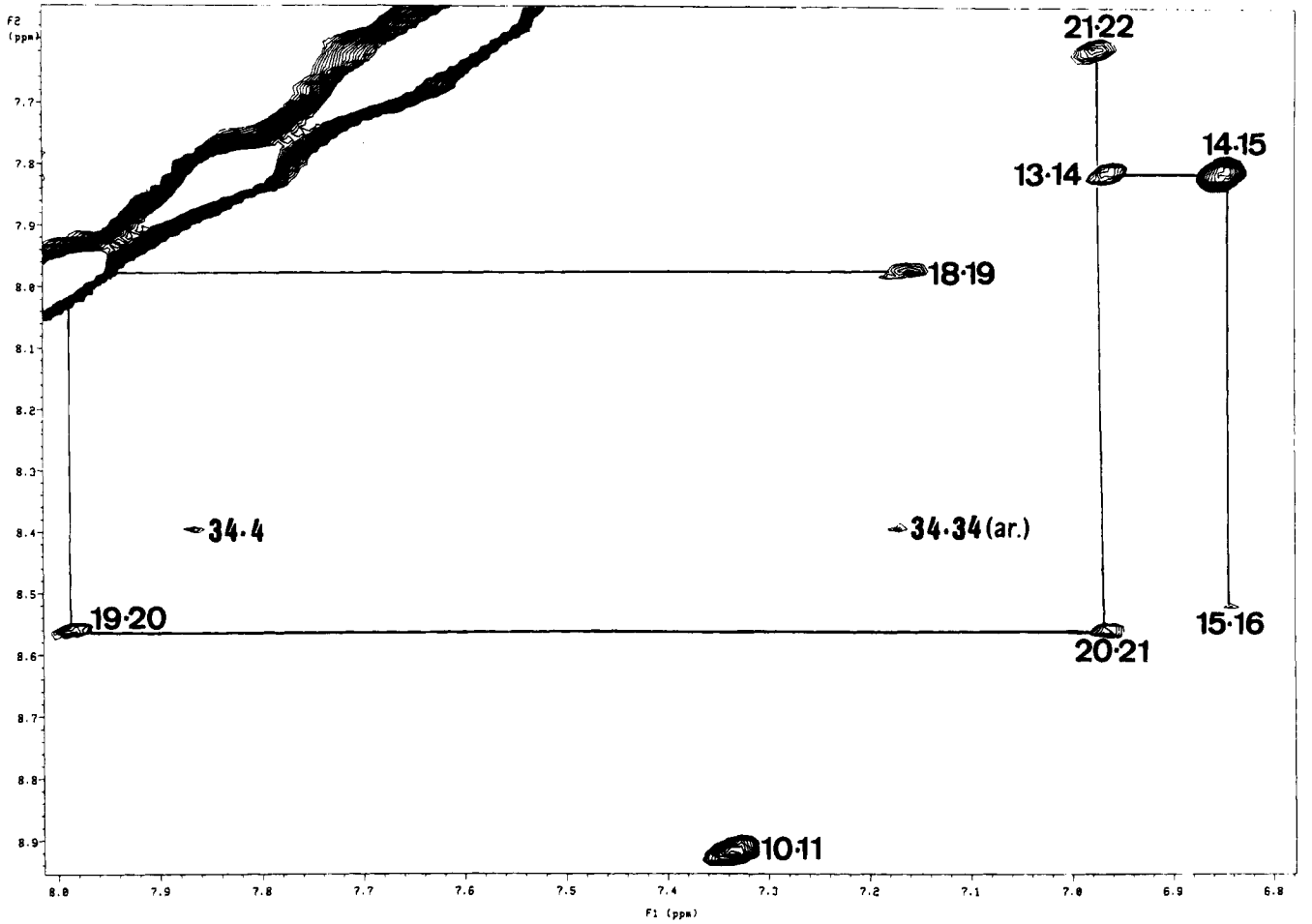

FIGURE 3: Expansion of a NOESY spectrum of KTX(1−37) showing the sequential NH-NH connectivities in the helical structure. The connectivity is broken by two prolines at positions 12 and 17. Experimental conditions are the same as in Figure 2, but the temperature is 25 °C.

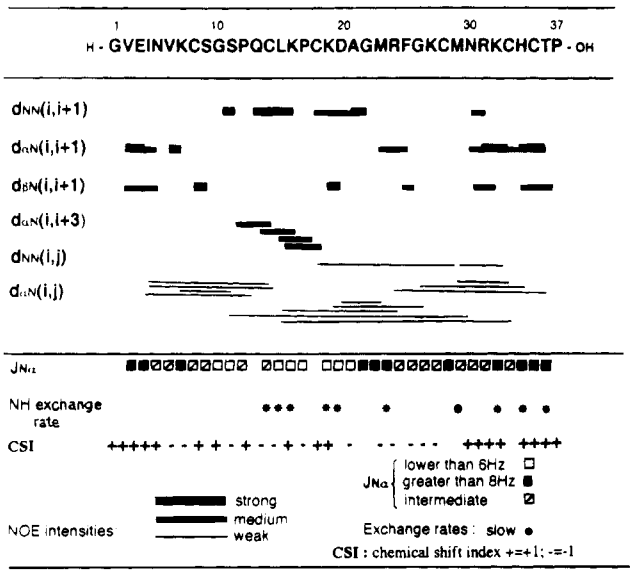

FIGURE 4: NMR data defining the secondary structure of kaliotoxin (1−37). The width of the lines indicating sequential or medium-range NOEs is proportional to the cross-peak intensity. Amide protons present in the spectrum after 7 h of exchange in D_2O are indicated as *. Small (<6 Hz) or large (>8 Hz) coupling constants are indicated by empty and filled squares, respectively. Chemical shift indexes (CSI) as defined in Wishart et al. (1992) are listed as + for +1 and − for −1.

be hydrogen bonded to the carbonyl oxygen of the residue situated in position *i*-4, i.e., forming the expected hydrogen bond for a pure α-helical structure. Finally, in the third set, the carbonyl oxygens supposed to be hydrogen bonded were chosen by assuming an α-helix from residues 12 to 17 and a 3_{10} helix from 18 to 20. This latter assumption was supported by the presence of an NOE *i*-*i*+2 in this region. The three sets afforded structures with the same overall fold and helical and β-sheet regions but the structures in the first and third sets showed the best agreement and the distances between carbonyl oxygens and amide protons found in the structures derived without hydrogen bond constraints were consistent with the presence of the 3_{10} helix from residues 18 to 20.

From the 50 resulting conformers in the third set, the 12 which best fitted the constraints were selected as input coordinates for simulated annealing calculations. The 12 structures had no violations of angular constraints larger than 20°. Six of them had no distance violation larger than 0.5 Å and the rest contained only one distance violation between 0.5 and 0.6 Å. The root mean square deviation (rmsd) of the backbone atoms of the 12 structures versus the average structure was 0.9 Å.

Previous to the refinement protocol, the three disulfide bonds which had been introduced simply as distance restraints were defined as covalent bonds. The simulated annealing protocol is defined in Table 2. Of the 12 final structures one showed the wrong configuration in one residue and was not considered for further analysis. The remaining set of structures had a rmsd value of 0.66 Å (backbone atoms)

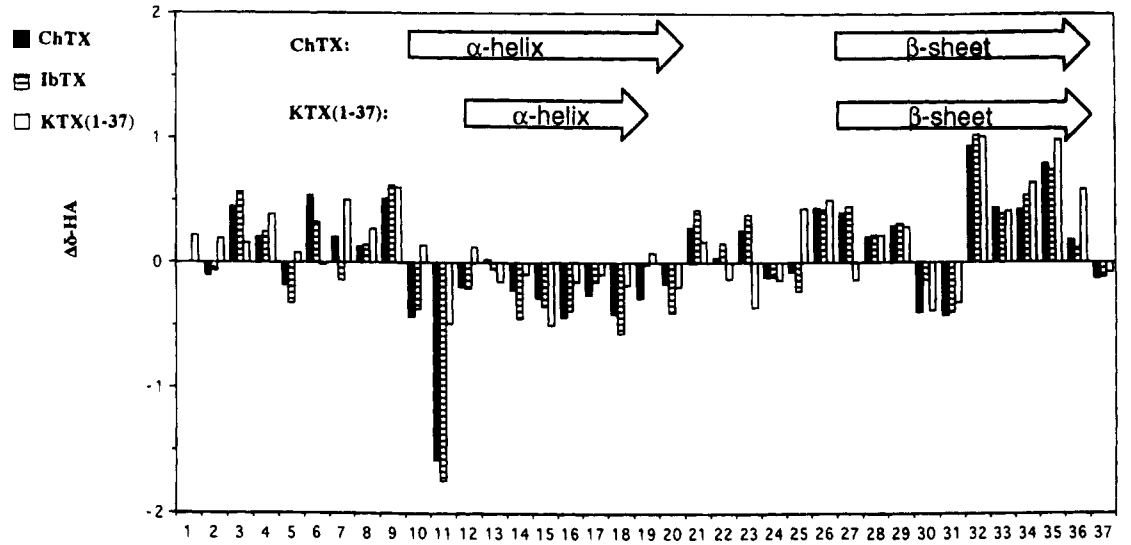

FIGURE 5: Conformational shifts of the α-protons of IbTX, ChTX, and KTX(1−37). Conformational shifts are deviations of the measured chemical shifts from the random-coil values listed in Wüthrich et al. (1986).

Table 1: Proton Chemical Shifts of KTX(1−37) at 35 °C and pH = 3.2[a]

amino acid	NH	Hα	Hβ	others
Gly1		4.38/4.03		
Val2	8.71	4.37	1.98	H^{γ} 0.91/0.98
Glu3	8.62	4.45	2.14/1.65	H^{γ} 2.00
Ile4	8.21	4.79	1.88	H^{γ} 1.21/1.04/0.81, H^{δ} 0.68
Asn5	8.70	4.83	2.94/2.64	H^{δ} 7.21
Val6	8.01	4.17	1.50	H^{γ} 0.88/0.94
Lys7	8.39	4.86	1.80	H^{γ} 1.72, H^{δ} 1.54, H^{ϵ} 3.03, H^{z} 7.52
Cys8	8.84	4.96	2.85/2.54	
Ser9	7.87	5.12	3.61	
Gly10	7.70	4.47/4.08		
Ser11	9.30	4.01	3.82	
Pro12		4.30	2.33/1.68	H^{γ} 2.12/2.31, H^{δ} 3.60/3.63
Gln13	7.34	4.22	2.59/2.43	H^{γ} 2.30, H^{ϵ} 7.30
Cys14	8.19	4.60	3.08/2.55	
Leu15	7.22	3.98	1.82/1.70	H^{δ} 0.96/1.05, H^{γ} 1.75
Lys16	8.90	4.20	1.96/1.90	H^{γ} 1.68, H^{δ} 1.40
Pro17		4.34	2.38/2.90	H^{γ} 2.18/2.04, H^{δ} 3.67/3.68
Cys18	7.53	4.51	3.06/2.96	
Lys19	8.35	4.44	1.92/1.57	H^{γ} 1.71, H^{ϵ} 3.04, H^{z} 7.76
Asp20	8.94	4.57	2.91/2.67	
Ala21	7.35	4.52	1.52	
Gly22	7.99	3.84/4.21		
Met23	8.06	4.10	2.21	H^{γ} 1.74/1.79
Arg24	9.35	4.24	1.78	H^{γ} 1.71, H^{δ} 3.02/2.93
Phe25	7.95	4.22	3.21/2.85	H2/H6 7.25, H4 7.31, H3/H5 7.36
Gly26	7.14	3.28/3.21		
Lys27	7.98	4.22	1.42	H^{γ} 1.86, H^{δ} 1.29, H^{ϵ} 3.02, H^{z} 7.60
Cys28	7.96	4.91	3.21/3.04	
Met29	8.76	4.80	2.24/1.43	H^{γ} 1.77
Asn30	9.44	4.37	3.05/2.78	H^{δ} 7.21
Arg31	8.54	4.06	2.28/2.31	H^{γ} 1.64/3.29, H^{δ} 3.24, H^{ϵ} 7.14
Lys32	7.78	5.37	1.93	H^{γ} 1.48/1.58, H^{δ} 1.72, H^{ϵ} 3.01, H^{z} 7.59
Cys33	8.41	5.10	2.69/2.56	
His34	9.53	5.27	3.15	H^{δ} 7.56, H^{ϵ} 8.76
Cys35	9.27	5.68	3.12/2.66	
Thr36	8.83	4.94	4.10	H^{γ} 1.36
Pro37		4.35	2.50/1.87	H^{γ} 2.14/2.04, H^{δ} 3.90/3.85

[a] Shifts were measured relative to dioxane.

and 1.73 Å (all atoms) versus the lowest energy structure and of 0.71 and 1.97 Å, respectively, between all the structures.

Order parameters were calculated for the dihedral angles ϕ and ψ as the sum of a vector of modulus one and a polar angle equal to the corresponding dihedral value (Hyberts et al., 1991); the results are presented in Figure 6. Values close to one indicate that the corresponding angle is well defined in all the structures. According to this criterion the backbone conformation is very well defined in all the molecules with the exception of the region around the β-turn that shows small variations.

The geometrical ideality and the occupation of the different Ramachandran regions were checked with the Procheck program (Laskowski et al., 1993) and were found to be correct except for residues ^{27}Lys, ^{29}Met, and ^{30}Asn which were outside the allowed regions of the Ramachandran map. Residues ^{30}Asn, ^{32}Lys, ^{34}His, and ^{12}Pro showed deviations from the ideal bond angles. These distortions could be removed by a short energy minimization, which however maintained the overall geometry (average rmsd backbone (10−37) between minimized and nonminimized structures is 1.5 Å). The affected residues are located in the β-turn and the adjacent region where the extended N-terminal region makes contact with the β-sheet.

Conformational shifts arising from amide bond anisotropy were calculated for the CHα protons (Herranz et al., 1992), and deviations from experimental values were found to be smaller than one standard deviation (as found in the calibration set) except for cysteines 14, 28, and 35 and Met 29.

Figure 7 shows a superposition of the backbone atoms of the 11 structures selected. Residues 1−8 form an extended structure followed by a loop that leads into an α-helix extending from residues 12 to 18. One turn of a 3_{10} helix and a second loop through residues 21−23 leads into the antiparallel sheet from 24 to 37. A turn from 29 to 32 separates the two antiparallel strands of the sheet. The helix is distorted in a bended conformation probably due to the presence of the two Pro residues. The helix and one face of the sheet are held in proximity by the two disulfides (14−33 and 18−35) facing each other. The axis of the helix is almost perpendicular to the β-sheet.

The structures have been deposited with the Protein Data Bank (Chemistry Department, Brookhaven National Laboratory, Upton, NY, 11973) under the filename 1KTX.

Table 2: Protocol Used for the Simulated Annealing Calculations

	DGII Structures
minimization	300 steps with descendant harmonic constraints = 1000 → 10 kcal·mol^{-1}·Å^{-2}, 600 steps of minimization without restraints
thermalization	20 cycles of 1000 steps, temperature = 0 → 1000 K, K(NOE) = 0.1 → 50 kcal·mol^{-1}·Å^{-2}, K(dihe) = 0.1 → 20 kcal·mol^{-1}·rad^{-2}, K(repel) = 0.01 kcal·mol^{-1}·Å^{-2}
equilibration	10 cycles of 1000 steps at 1000 K, K(repel) = 0.01 → 4 kcal·mol^{-1}·Å^{-4}, 50 cycles of 1000 steps of equilibration
cooling	50 cycles of 1000 steps, temperature = 1000 → 0 K
minimization	600 steps at temperature = 0 K, K(NOE) = 50 kcal·mol^{-1}·Å^{-2}, K(dihe) = 20 kcal·mol^{-1}·rad^{-2}, K(repel) = 4 kcal·mol^{-1}·Å^{-4}
final structures	

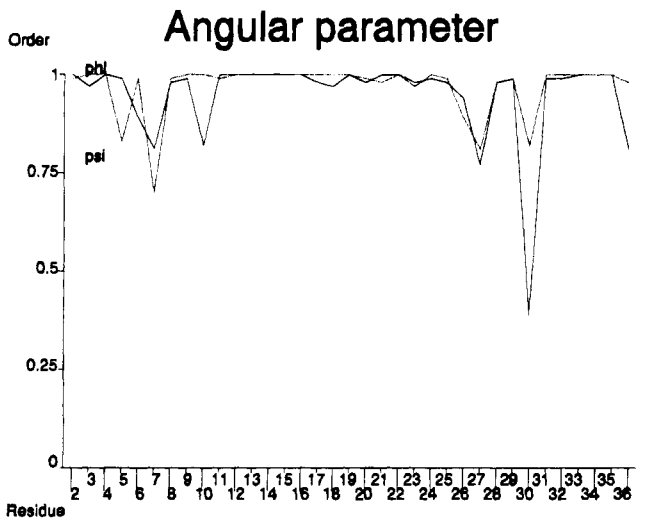

FIGURE 6: Angular order parameters for the main-chain angles ϕ and φ in the 11 final structures of KTX(1−37).

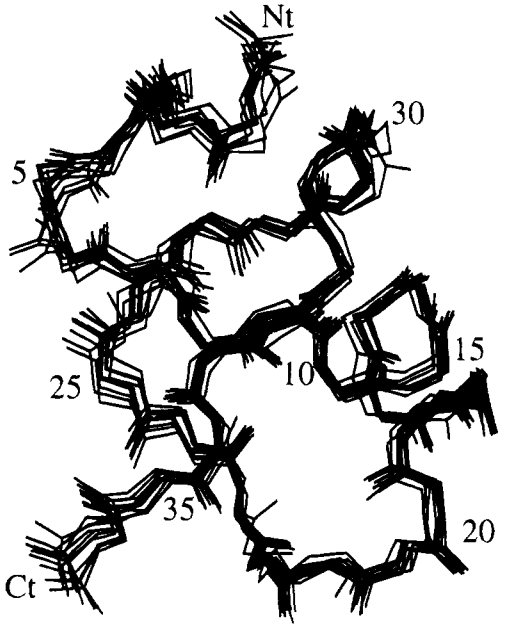

FIGURE 7: Backbone superposition of the 11 refined structures of KTX(1−37). The rmsd of this set is 0.66 Å (backbone) and 1.77 Å (all atoms) with respect to minimum energy structure.

DISCUSSION

The structure of KTX(1−37) in solution is very well defined and shows the same basic structural motif found in ChTX and IbTX (Bontems et al., 1991, 1992; Johnson et al., 1992), as expected from the sequence homology and the common disulfide bond pattern. In particular the same sequence of secondary structure elements are found in the three toxins. The overall structural similarity between these three toxins is reflected in the similar profile of chemical shifts observed (Figure 5). This chemical shift profile relates to the observed secondary structure (Ösapay et al., 1991).

In spite of these similarities a number of differences between the structures are apparent and they will be discussed in detail. An area of special interest in KTX(1−37) is the helical region because of the presence of two Pro residues that were expected to introduce large distortions. In fact, the first proline (^{12}Pro) determines the beginning of the helix and therefore causes a reduction of the helix length by two residues as compared to charybdotoxin. The second (^{17}Pro) does not cause a total termination of the helical part of the molecule but introduces some distortions. Most notably a bending of the helical axis and a change in pitch of the helix following ^{17}Pro from an α-helix to a 3_{10} helix. Proline has been shown to cause bending in helices (Piela et al., 1987); this effect facilitates the compensatory hydrogen bonding between solvent and the carbonyl oxygen of residues i-3 or i-4 from Pro (Woolfson et al., 1990); indeed we have found the carbonyl group from residues 13 and 14 exposed to solvent in the structure of KTX(1−37). The degree of bending, as compared to ChTX, was quantified by superimposing the first residues of the KTX(1−37) helix (12−15) to the homologous residues in ChTX and measuring the distance between the centers of the last turn of the two helices, residues 18−20 of KTX(1−37) and 19−21 of ChTX which was found to be 5 Å. Three points located at the center of the helix turns involving residues 12−15, 15−17, and 18−20 formed an angle of 40°. Recent calculations have shown that the presence of Pro is not as unfavorable for helix formation as previously believed (MacArthur et al., 1991; Yun et al., 1991; Polinsky et al., 1992).

The presence of a 3_{10} helix in the terminal part of the helix in KTX(1−37) is supported by the calculations made without hydrogen bonds and also by the presence of a (i, i+2) NOE between residues 18 and 20. 3_{10} helices are often found in short stretches at the end of α-helical regions. In the present case, if the helical region is expected to terminate at the same position as in ChTX, the number of residues after ^{17}Pro is not sufficient to allow a complete α-helix turn but can still accommodate a 3_{10} turn.

The region from 25 to 36 forms a hairpin structure of the same length as that of IbTX, but longer than that of ChTX (26−35). This region is probably involved in binding as it has been shown that a peptide with the sequence 26−32 and 25−35 of KTX(1−37) competes with the full molecule for its binding site and is able to antagonize KTX in both its toxicity and blocking activities (Romi et al., 1993). For the three toxins, the relative orientation of the residues on strands (25−28 and 33−36) of the β-sheet are identical but superposition of the hairpins of KTX(1−37) and ChTX is not perfect: if the C-terminal strands are aligned, the 25−29 strand of KTX(1−37) forms a 30° angle with the corresponding strand of ChTX.

The turn region is the less well defined in the structure of KTX(1−37). The NH-CHα and NH-NH NOEs qualitatively suggest a type I β-turn, but this appears highly distorted in the final structures. One possible reason may be the presence of multiple local conformations. The presence of ^{30}Asn in the i+2 position of the turn flanked by two polar residues suggests that a Asx-turn (Abbadi et al., 1991) may be in equilibrium with the β-turn. The most populated rotamer around the Cα−Cβ bond of Asn, as measured from the coupling constant between the α and β protons, is g^- in agreement with expectations if an Asx turn were to be significantly populated in the equilibrium.

The conformations found for the disulfide bonds were studied from its χ_i dihedral angles. Several disulfide bridge conformations can be accommodated by the global protein fold. χ_i are well defined by the measured NOEs and coupling constants, and the different disulfide bond conformations arise from variations in the χ_2 and the χ_{ss} angles. Both P and M chirality are observed in different structures. The dihedral angle $/\chi_{ss}/$ is around 90° for the disulfide bond between 8−28 and 18−35 but deviates significantly from 90° for the disulfide bond between cysteines 14−33. A similar situation is found in charybdotoxin with a lack of definition in the conformation of the disulfide bonds and significant deviations from 90° for χss in the disulfide bond between cysteines 13−33.

The NMR structure was compared to a model derived from the known structure of ChTX by mutation and energy minimization and the two structures were found to have a very poor superposition (backbone rmsd = 6.63 Å). The reason for this discrepancy comes from a difference in the global folding of KTX(1−37) and ChTX affecting the location of the β-sheet with respect to the helix and the N-terminal region. This is shown schematically in Figure 8a,b). While the N-terminal region of KTX(1−37) wraps around the face of the β-sheet opposite the one that is in contact with the helix, in ChTX this N-terminal region and the α-helix interact with the same face of the β-sheet. This difference in folding is experimentally supported by a number of NOEs involving side chains in the β-sheet region of KTX-(1−37) that indicate that one face of the β-sheet is in contact with the helix and the other with the N-terminal strand. The different folding of KTX(1−37) and ChTX is a consequence of the changes in the helical region caused by the presence of prolines in KTX(1−37). As mentioned before, ^{12}Pro in KTX(1−37) causes a shortening of the helix and therefore a lengthening of the extended N-terminal region that precedes it. The bending of the helix caused by ^{17}Pro also helps to facilitate the wrapping of the N-terminal segment around the side of the β-sheet opposite to the one in contact with the helix.

The folding found in KTX(1−37) affects the accessibility of ^{27}Lys. This residue also shows a low order parameter and lies outside the regions normally allowed in the Ramachandran map in some of the refined structures.

In order to quantify the exposure of the positive charge of ^{27}Lys in KTX(1−37) and ChTX, we carried out electrostatic calculations on a representative structure for each toxin using Delphi. The quantity of interest is the reaction field energy which is a measure of the solvent response to the charges in the molecule and therefore it is expected to be sensitive to the accessibility of the solvent to the different charged residues. We have calculated the electrostatic

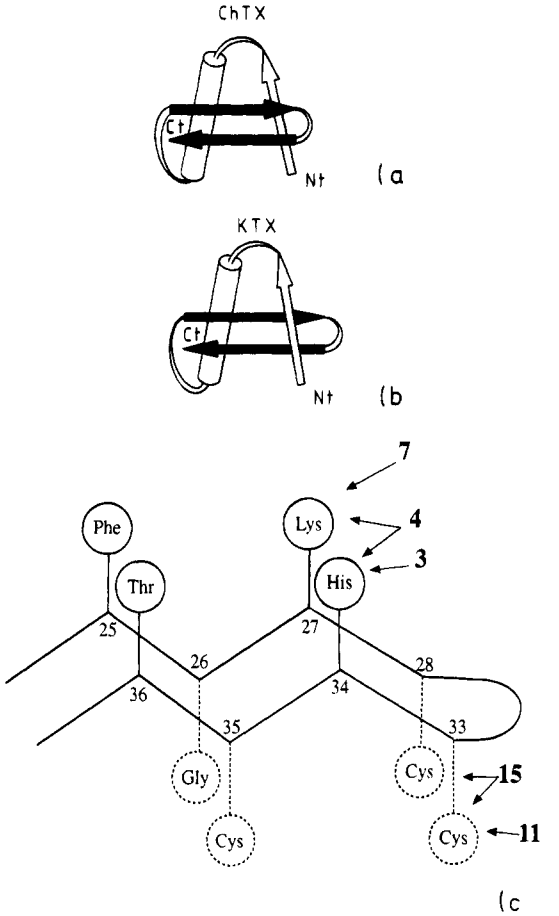

FIGURE 8: Idealized drawing of the folding of ChTX (a) and KTX-(1−37) (b). The helix is represented by a cylinder and the extended strands as straight arrows. The main difference between the two foldings is that in KTX(1−37) the N-terminal strand and the α-helix interact with opposite sides of the β sheet. This is directly supported by the NOEs involving side chains that are oriented to either side of the β sheet indicated in (c), where the numbers in boldface correspond to the residues that show at least a NOE to the indicated side chain.

reaction field energy for KTX(1−37) and ChTX with a single charge located in the side chain of different Lys residues. For KTX(1−37) the reaction field energy calculated with a single charge located on ^{27}Lys is 1.8 kcal mol^{-1} higher than that obtained when the charge is located on ^{32}Lys, a well-exposed residue in both KTX and ChTX. For ChTX the difference in the corresponding reaction field energies is only of −0.1 kcal mol^{-1}. The difference found in KTX(1−37) indicates a lower interaction of the charge in ^{27}Lys with its image induced on the surface of the molecule as a consequence of the lower exposure of this residue.

Mutational studies in ChTX have shown that ^{27}Lys is one of the essential residues for tight binding to the channel receptor (Park et al., 1992). This residue is also part of the sequence 26−32 of KTX which has been shown to inhibit KTX binding to its receptor.

Delphi calculations using all formal charges also provide a representation of the potential at the surface of the molecule that shows, in both cases, two faces with different signs. This electrostatic asymmetry is very similar in KTX(1−37) and ChTX and gives rise to a largely positively charged face, as expected from their net positive charge, that is supposed to interact with the receptor as postulated by (Johnson et al., 1992).

The differences observed in the conformation of KTX and ChTX or IbTX may be the origin of the relative specificity of action as observed clearly in various systems. For example, on calcium-activated large-conductance potassium channels from skeletal muscles, ChTX and IbTX show high activity compared to KTX (IC_{50} 400 μM; Crest, personal communication). This weak affinity may be related to the high value of the k_{off} observed compared to that of ChTX and IbTX (Crest, personal communication). Furthermore, KTX is much more active than ChTX and IbTX (IC_{50} of KTX 10 pM, IC_{50} of ChTX 8 nM, and >μM for IbTX) in voltage-dependent potassium channels (sensitive to dendrotoxin) in rat brain synaptic membranes (Romi et al., 1993). On the other hand, one can observe that all toxins (NTX, MgTX, TsKα, and KTX) containing proline residues in the α-helix region of ChTX or IbTX exhibit a high blockage activity of voltage-dependent potassium channels.

These differences in biological activity and the structural data presented in this paper suggest that KTX and probably other proline-containing toxins of this family represent a different subfamily of toxins active in voltage-dependent potassium channels.

ACKNOWLEDGMENT

We wish to thank Drs. M. Crest and F. Sampieri for fruitful discussions. This work has been carried out using the NMR facility which is part from the Serveis Científics i Tècnics of the University of Barcelona.

REFERENCES

Abbadi, A., Mcharfi, M., Aubry, A., Prémilat, S., Boussard, G., & Marraud, M. (1991) *J. Am. Chem. Soc. 113*, 2729−35.

Bontems, F., Roumestand, C., Boyot, P., Gilquin, B., Doljansky, Y., Ménez, A., & Toma, F. (1991) *Eur. J. Biochem. 196*, 19−28.

Bontems, F., Gilquin, B. Roumestand, C., Ménez, A., & Toma, F. (1992) *Biochemistry 31*, 7756−64.

Braunschweiler, L., & Ernst, R. R. (1983) *J. Magn. Reson. 53*, 521−58.

Crest, M., Jacquet, G., Gola, M., Zerrouk, H., Benslimane, A., Rochat, H., Mansuelle, P., & Martin- Eauclaire, M-F. (1992) *J. Biol. Chem. 267*, 1640−47.

Davis, D. G., & Bax, A. (1985) *J. Am. Chem. Soc. 107*, 2820−21.

Feinstein, R. D., Polinsky, A., Douglas, A. J., Magnus, C., Beijer, C. F., Chadha, R. K., Benedetti, E., & Goodman, M. (1991) *J. Am. Chem. Soc. 113*, 3467−73.

Fontecilla-Camps, J-C., Almassy, R. J., Suddath, F. L., Watt, D. D., & Bugg, C. (1980) *Proc. Natl. Acad. Sci. U.S.A. 77*, 6496−500.

Fontecilla-Camps, J-C., Habersetzer-Rochat, C., & Rochat, H. (1988) *Proc. Natl. Acad. Sci. U.S.A. 85*, 7443−47.

Galvez, A., Gimenez-Gallego, G., Reuben, J. P., Roy-Contancin, L., Feigenbaum, P., Kaczorowski, G. J., & García, M. L. (1990) *J. Biol. Chem. 265*, 11083−90.

García-Calvo, M., Leonard, R. J., Novick, J., Stevens, S. P., Schmalhofer, W., Kaczorowski, G. J., & García, M. L. (1993) *J. Biol. Chem. 268*, 18866−74.

Gilson, M., & Honig, B. (1988) *J. Comput. Chem. 9*, 327−37.

Gimenez-Gallego, G., Navia, M. A., Reuben, J. P., Katz, G. M., Kaczorowski, G. J., & García, M. L. (1988) *Proc. Natl. Acad. Sci. U.S.A.* 85, 3329−33.

Habermann, E. (1984) *Pharmacol. Ther. 25*, 255−70.

Harvey, A. L., Vantapour, H., Rouvan, E. G., Pinkasfeld, S., Vita, C., Ménez, A., & Martin-Eauclaire, M-F. (1994) *Toxicon* (in press).

Herranz, J., González, C., Rico, M., Nieto, J. L., Santoro, J., Jiménez, M. A., Bruix, M., Neira, J. L., & Blanco, F. J. (1992) *Magn. Reson. Chem. 30*, 1012−18.

Hyberts, S. G., Goldberg, M. S., Havel, T. F., & Wagner, G. (1992) *Protein Sci. 1*, 736−51.

Jeener, J., Meier, B. H., Bachman, P., & Ernst, R. R. (1979) *J. Chem. Phys. 71*, 4546−53.

Johnson, B. A., & Sugg, E. E. (1992) *Biochemistry 31*, 8151−59.

Kobayashi, Y., Takashima, H., Tamaoki, H., Kyogoku, Y., Lambert, P., Kuroda, H., Chino, N., Watabane, T. X., Kimura, T., Sakakibara, S., & Moroder, L. (1991) *Biopolymers 31*, 1213−20.

Krishna, N. R., Moore, C. H., Narasimhan, S., & Watt, D. D. (1990) *Peptides: Chemistry, Structure and Biology* (Rivier, J. E., & Marshall, G. R., Eds.) pp 625−627, ESCOM, Leiden, The Netherlands.

Laskowski, R. A., MacArthur, M. W., Moss, D. S., & Thornton, J. M. (1993) *J. Appl. Crystallogr. 26*, 283−91.

MacArthur, M. W., & Thornton, J. M. (1991) *J. Mol. Biol. 218*, 397−412.

Macura, S., Huang, Y., Suter, D., & Ernst, R. R. (1981) *J. Magn. Reson. 43*, 259−81.

Ösapay, K., & Case, D. (1991) *J. Am. Chem. Soc. 113*, 9436−44.

Park, C-S., & Miller, C. (1992) *Biochemistry 31*, 7749−55.

Piela, L., Némethy, G., & Scheraga, H. A. (1987) *Biopolymers 26*, 1587−600.

Polinsky, A., Goodman, M., Williams, K. A., & Deber, C. M. (1992) *Biopolymers 32*, 399−406.

Rance, M., Sørensen, O. W., Bodenhausen, G., Wagner, G., Ernst, R. R., & Wüthrich, K. (1983) *Biochem. Biophys. Res. Commun. 117*, 479−85.

Rogowsky, R. S., Krueger, B. K., Collins, J. H., & Blaustein, M. P. (1994) *Proc. Natl. Acad. Sci. U.S.A. 91*, 1475−79.

Romi, R., Crest, M., Gola, M., Sampieri, F., Jacquet, G., Zerrouk, H., Mansuelle, P., Sorokine, O., Van Dorsselaer, A., Rochat, H., Martin-Eauclaire, M-F., & Van Rietschoten, J.(1993) *J. Biol. Chem. 268*, 26302−09.

Srinivasan, N., Sowdhamini, R., Ramakrishnan, C., & Balaram, P. (1990) *Int. J. Pept. Protein Res. 36*, 147−55.

Sugg, E. E., García, M. L., Reuben, J. P., Patchett, A. A., & Kaczorowski, G. J. (1990) *J. Biol. Chem. 265*, 18745−48.

Wishart, D. S., Sykes, B. D., & Richards, F. M. (1992) *Biochemistry 31*, 1647−51.

Woolfson, D. N., & Williams, D. H. (1990) *FEBS Lett. 277*, 185−88.

Wüthrich, K. (1986) *NMR of Proteins and Nucleic Acids*, J. Wiley and Sons, New York.

Yun, R. H., Anderson, A., & Hermans, J. (1991) *Proteins 10*, 219−228.